Effect of carrier gas on copper antimony sulfide thin films by spray pyrolytic approach

Y. B. Kishore Kumar[a], S. Guru Prasad[b], A. S. Swapna Smitha[c], U. Chalapathi[d,*], G. Suresh Babu[c], Y. Jayasree[e], P. Uday Bhaskar[f], Si-Hyun Park[d]
[a]*Solar Energy Laboratory, Mohan Babu University (Erstwhile Sree Vidyanikethan Engineering College), Tirupati-517102, India*
[b]*Department of Physics, N.T.R. Government Degree College, Vayalpad-517299, India*
[c]*Department of Physics, Government Degree College, Puttur-517583, India*
[d]*Department of Electronic Engineering, Yeungnam University, 280 Daehak-Ro, Gyeongsan, Gyeongbuk, 38541, South Korea*
[e]*Department of Physics, S.P.W. Degree and PG College, Tirupati-517502, India*
[f]*National Institute of Solar Energy, Gwal Pahari, Haryana and Mundra Solar Technology LTD (Adani Solar), Mundra, Gujarat-370435, India*

This study explores the ternary compound semiconductor as a potential absorber layer for third-generation solar cells. $CuSbS_2$, a promising candidate for thin film absorber layers, is fabricated using a simple spray pyrolysis method. The research specifically investigates the influence of two different carrier gases during the fabrication process. X-ray diffraction as well as Raman studies confirm that the films exhibit a chalcostibite structure. Notably, films fabricated with nitrogen as the carrier gas demonstrate enhanced crystallinity, accompanied by reduced microstrain and dislocation density. Furthermore, these films exhibit a significantly improved absorption coefficient, reaching 10^5 cm^{-1}. Optical studies indicate that the materials possess a direct band gap of 1.50 eV and exhibit p-type conductivity. $CuSbS_2$ thin film heterojunction solar cell exhibits a maximum efficiency of 0.49%.

(Received June 27, 2024; Accepted September 12, 2024)

Keywords: $CuSbS_2$, Thin films, Spray pyrolytic technique, Carrier gases, Solar cell

1. Introduction

With an increase in the population of any country, the usage of electricity as well as pollution increases. The security and economy of every nation critically rely on the electricity available in that country. For power production, the majority of nations strongly depend on fossil fuels, which cause greenhouse gases as well as other pollutants that cause climate change. However, the available fossil fuels may drain in the upcoming days [1]. Hence indeed to search for an alternative to this method. In this scenario, renewable energy sources are one of the best alternatives to any method. Inexhaustible and pollution-free solar energy is one of the most promising alternative energy sources for tropical nations like India. Thin film solar cells, which provide affordable, adaptable, and eco-friendly energy generation solutions, are essential to the widespread utilization of solar energy. $Cu(In,Ga)Se_2$, CdTe, and $Cu_2ZnSn(S,Se)_4$ thin film solar cells exhibited record efficiency of 23.35%, 22.6%, and 14.9%, individually [2,3]. But, the elements Cd, Te, and Se are naturally hazardous, In and Ga are scarce elements, these reasons minimize their commercial values.

As a remade of above said limitations, copper (Cu) antimony (Sb) sulfide (S) (I-V-VI_2) chalcogenide semiconducting materials emerged as an alternative potential photovoltaic solar cell [4]. This semiconducting material consists of abundant, un-hazardous, and low-cost constituent elements. $CuSbS_2$ thin films are well suitable for an absorber layer in thin film solar cells owing to their significant properties such as large optical absorption coefficient, a direct band gap nature (≈

* Corresponding authors: chalam.uppala@gmail.com
https://doi.org/10.15251/CL.2024.219.719

1.5 eV), chalcostibite structure, and p-type conductivity [5,6], which align closely with the ideal standards for PV applications.

These ternary films were deposited by Banu et al. using hybrid inks, and they achieved a record efficiency of 3.22% [7]. Chalapathi et al. [8] achieved a maximum efficiency of 2.2 % as they deposited these films via sulfurization in stacks. $CuSbS_2$ thin films were grown by various physical as well as chemical methods like atomic layer deposition [9], co-sputtering [10], rapid thermal processing [11], thermal evaporation [12], two-stage processes [13], hot injection [14], CBD approach [15], spin coating [16], electrodeposition [17], and spray pyrolytic approach [18].

Out of these approaches, spray pyrolysis is a trouble-free, economical method that could be used for large-scale production. Spray pyrolysis process parameters include the substrate surface temperature, distance between nozzle and substrate, additives, duration of deposition, solution flow rate, pH value, and viscosity of the precursor solution [19,20]. Compressed air has often been utilized in spray pyrolysis as a carrier gas. This study investigates the effects of nitrogen as well as compressed air as carrier gas on the fabrication of $CuSbS_2$ thin film. For the 1st time, the studies on $CuSbS_2$ thin films utilizing nitrogen as the carrier gas were reported.

While depositing these $CuSbS_2$ films, a small variation in the experimental circumstances causes the ternary impurity phase, such as Cu_3SbS_3, $Cu_{12}Sb_4S_{13}$, and binary phase, such as Cu_xS, Sb_2S_3, to be formed along with $CuSbS_2$ films [8,21,22]. In this study, an attempt was made to deposit these $CuSbS_2$ films in an inert atmosphere to reduce these impurity phases. Nitrogen gas was employed in spray pyrolysis as the carrier gas to provide an impurity-free atmosphere. This atmosphere could change the sprayed material's chemical composition or structure [23]. The resulting, phase of pure $CuSbS_2$ films might be formed which enhances the efficacy of the $CuSbS_2$ solar cells.

2. Experimental

$CuSbS_2$ thin films were fabricated by the spray pyrolytic approach. The salts of cupric chloride (0.01M), antimony tri chloride (0.01M), and thiourea (0.08M) were present in the starting solution [24,25]. To mitigate sulfur loss in pyrolysis, the concentration of thiourea salt in the precursor solution was retained above the stoichiometric value throughout the experiment [26]. The concentration of the salts was kept low in the current study to reduce viscosity in the starting solution, which produces smaller, more even droplets, which favours the deposition of thin films. The pH of the salt solution was maintained at about 3.5 [25]. After the glass substrate had been thoroughly cleaned, the salt solution was sprayed over it at a rate of 10 millilitre's per minute [27] at an optimal substrate surface temperature of 533 K [24,25]. $CuSbS_2$ films were deposited using nitrogen and compressed air as carrier gases and their results were compared. The spray system (Model: ¼ JAU, USA) and the high-temperature digital controller connected to the electric heater were housed in the fume hood which contains a high-speed exhaust fan.

Bruker X-ray diffractometer (XRD) and micro Raman spectra were used for the structural characterization. XRD patterns were recorded with Cu-Kα radiation. The Raman spectra were captured with a conventional green laser. The Jeol scanning electron microscope has been utilized to capture the morphological images. Transmittance spectra of the obtained films were measured with a Jasco double-beam spectrophotometer. Hall Effect as well as van der Pauw techniques were employed to study the electrical analysis. To conclude the type of conductivity of the sprayed films, the hot probe method was employed.

3. Results and discussion

With nitrogen and compressed air as carrier gases, the $CuSbS_2$ films were formed with remarkable homogeneity and adhered to the substrates. These films' elemental composition was identified using an energy-dispersive spectrometer and was presented in Table 1. The elemental composition results indicate the carrier gas had an impact on the deposited films. When nitrogen served as the carrier gas, the sulfur/(metal) ratio was approximately unity which is advantageous for

the fabrication of $CuSbS_2$ films. Also, a significant variation in the atomic percentage of copper and antimony in the film. The concentration of copper in the films was reduced which is favourable condition for minimizing the impurity phase in the films [22,28].

Table 1. Elemental analysis of sprayed $CuSbS_2$ films obtained from two carrier gases.

Carrier gas	Elemental composition (at %)			$\frac{Cu}{Sb}$	$\frac{S}{(Cu+Sb)}$
	Cu	Sb	S		
Compressed air	28.03	22.85	49.12	1.23	0.96
Nitrogen	26.87	23.41	49.72	1.15	0.99

Fig.1 illustrates the XRD spectra of deposited $CuSbS_2$ films by employing compressed air as well as nitrogen as carrier gases. The films deposited with two distinct carrier gasses indicated an orthorhombic system with a chalcostibite structure [29,30]. The deposited films were orientated in the desirable (111) crystal plane in both instances. Films fabricated using air as the carrier gas showed the $Cu_{2-x}S$ phase [31]. This $Cu_{2-x}S$ impurity phase has vanished in the $CuSbS_2$ films obtained by utilizing nitrogen (N_2) as the carrier gas. Additionally, the $I_{(111)}/I_{(020)}$ intensity ratio increased, indicating an improvement in the films' crystallinity [27]. This could be attributed to the ratio between the value of nitrogen gas weight to the volume of the salt solution was minimal when it was compared to the ratio of the weight of compressed air to the volume of the salt solution. [23,32].

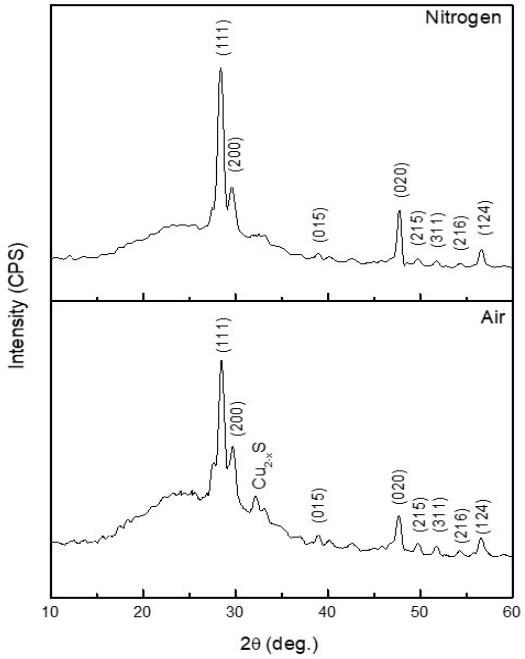

Fig. 1. X-ray diffraction spectra of $CuSbS_2$ films fabricated from two different carrier gases.

Using the XRD data, the following calculations have been made [33] and the obtained values are shown in Table 2. The lattice parameters of these films fabricated under two different carrier gases were assessed using the formula.

$$\frac{1}{d} = \sqrt{\frac{h^2}{a^2} + \frac{k^2}{b^2} + \frac{l^2}{c^2}} \quad (1)$$

In this context, d denotes the interatomic separation, (hkl) signifies Miller-indices of the corresponding lattice plane while a,b,c represent the lattice parameters.

$$\text{Crystallite size (D)} = \frac{0.94\,\lambda}{\beta\cos\theta} \quad (2)$$

where λ represents the wavelength of the X-ray source (0.1541 nm), β represents the full-width at half-maximum, and θ represents the Bragg angle.

$$\text{Microstrain } (\varepsilon) = \frac{\beta\cos\theta}{4} \quad (3)$$

$$\text{Dislocation density} = \frac{1}{D^2} \quad (4)$$

Table 2. XRD studies of various crystalline parameters of $CuSbS_2$ films obtained from two carrier gases.

Carrier gas	Lattice parameters (nm)			D (nm)	ε (10^{-3})	Dislocation density (10^{-3})
	a	b	c			
Compressed air	0.5978	0.3801	1.4528	22.46	1.6065	1.9823
Nitrogen	0.5996	0.3802	1.4506	27.60	1.3107	1.3127

The obtained lattice constants closely matched the reported values [29,30]. The utilization of nitrogen as the carrier gas led to a reduction in both the microstrain as well as the dislocation density within the films. Enhanced crystallinity in the films typically suggests a lower dislocation density [34,35]. This condition is favourable for efficient solar cells.

Raman spectroscopic studies can confirm the formation of the $CuSbS_2$ phase and assess its purity. Micro Raman spectrograph of $CuSbS_2$ thin films fabricated under two dissimilar carrier gases was illustrated in Fig.2. The Raman spectrum reveals significant peaks at 331 and 332 cm^{-1}, affirming the occurrence of the $CuSbS_2$ phase, and this was consistent with previous observations [25,36]. Although $Cu_{2-x}S$ appears as an impurity phase in the XRD spectra of films fabricated with air as a carrier gas, Raman's studies did not disclose any peaks corresponding to $Cu_{2-x}S$. This discrepancy may arise from the $Cu_{2-x}S$ phase lying just beneath the probe depth [22,37].

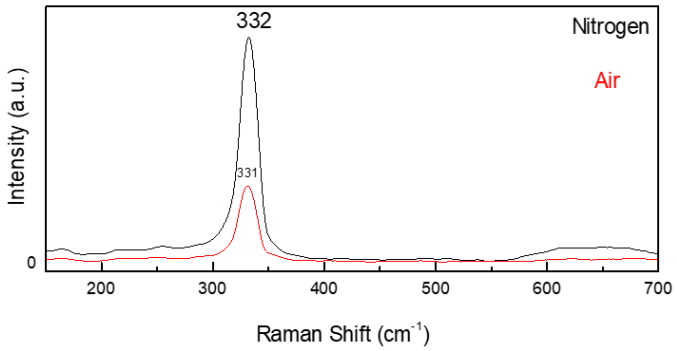

Fig. 2. Raman-spectra of $CuSbS_2$ films fabricated from two dissimilar carrier gases.

Fig. 3 displays the scanning electron micrograph image of $CuSbS_2$ thin films fabricated under two distinct carrier gases. SEM images indicated that the selection of carrier gas influenced the grain sizes. Films were fabricated using N_2 as the carrier gas, the grains exhibited uniform spacing as well as tight arrangement on the surface. This could be attributed to the ratio between the value of nitrogen gas weight to the volume of the salt solution was minimal, resulting in smaller aerosol sizes in contrast to compressed air. Moreover, nitrogen gas lacks moisture content, which could further enhance the film's morphology [38]. A compact surface morphology is pivotal for an absorber layer in PV applications [39].

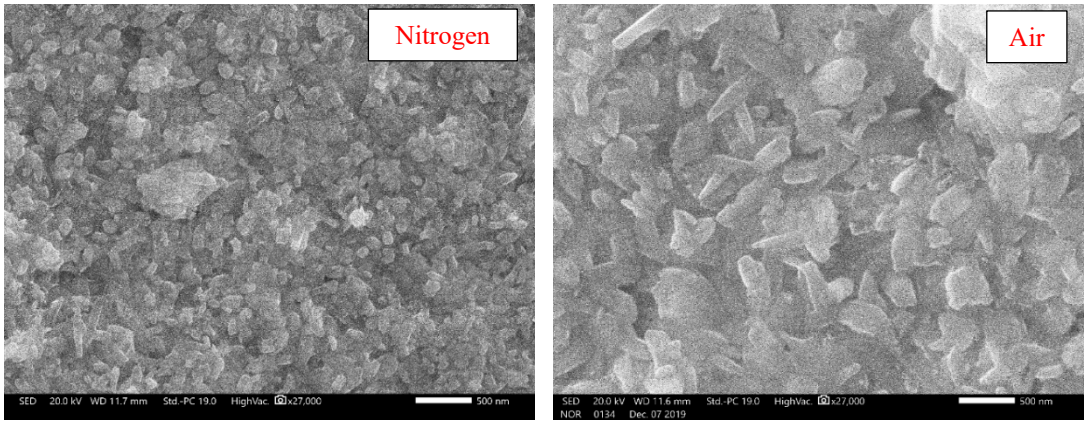

Fig. 3. SEM images showcasing $CuSbS_2$ films fabricated from two different carrier gases.

$CuSbS_2$ thin films were analyzed to determine their optical absorption coefficient (α) as well as the energy gap of the films fabricated under different carrier gases by examining their spectral transmittance curves. Fig. 4 illustrates the transmittance curves of $CuSbS_2$ films deposited under two carrier gases. When nitrogen was used, the transmittance spectra shifted towards shorter wavelengths. Additionally, there was a noticeable rapid decline in the transmittance curve at the vicinity of the fundamental absorption edge, suggesting a direct photo transition. α of the fabricated films was calculated utilizing the formula $\ln\left(\frac{[1-R]^2}{T}\right).\frac{1}{t}$, where R represents reflectance, T signifies transmittance, and t denotes the film thickness [26].

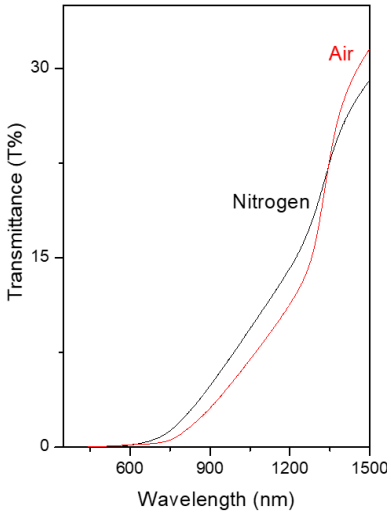

Fig. 4. Spectral transmittance of $CuSbS_2$ films fabricated from two carrier gases.

Fig. 5 shows the absorption coefficients of the deposited film by employing nitrogen as a carrier gas, which were found to exceed 10^5 cm^{-1}. Furthermore, the expression $(\alpha h\nu) = A(h\nu - E_g)^{1/2}$ interprets the absorption mechanism as direct transitions and A represents a constant [26]. The intersection of the (hν) versus $(\alpha h\nu)^2$ provides the band gap, as illustrated in Fig. 6, which exhibits a linear fit indicative of direct optical transitions. The band gap of $CuSbS_2$ films grown with two carrier gases was found to be 1.42 eV and 1.50 eV correspondingly [22]. A significant enhancement in the band gap was noted when N_2 was used. The enhancement value closely aligns with the optimal energy gap corresponding to the solar energy spectrum.

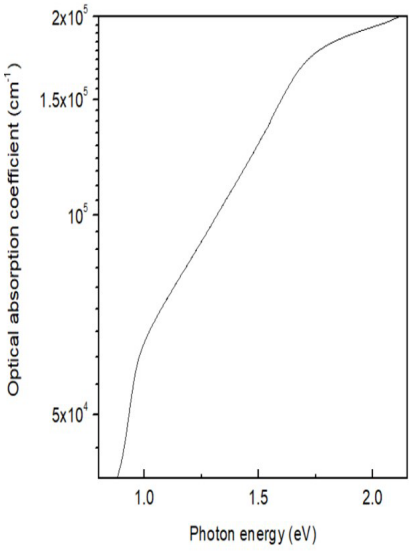

Fig. 5. Optical absorption coefficient spectrum of $CuSbS_2$ films.

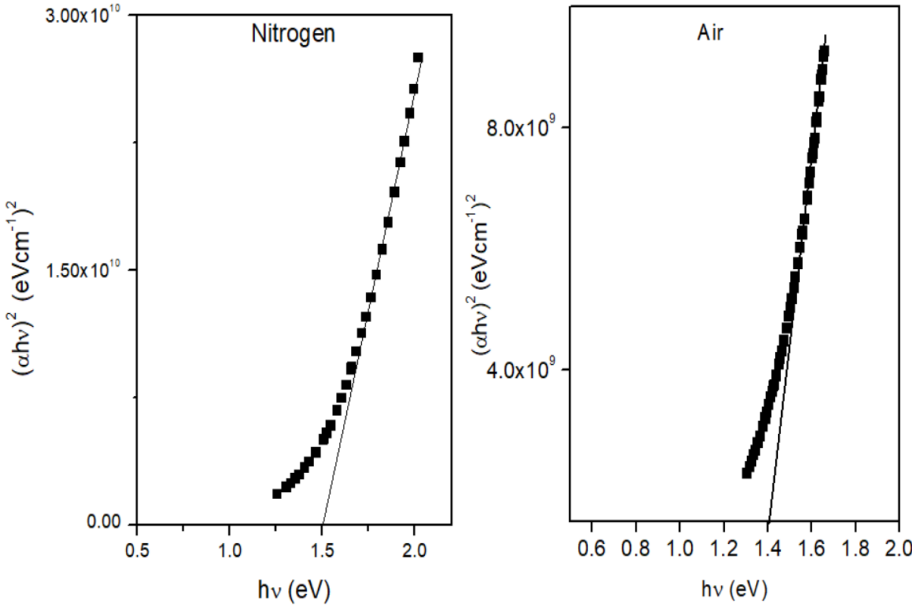

Fig. 6. Energy gap of $CuSbS_2$ films fabricated by using two different carrier gases.

The room temperature electrical resistivity of the films was examined by the van der Pauw method, yielding a value of 10 Ω cm. Additionally, the films demonstrated a Hall mobility of 1.13 cm^2/Vs. The carrier concentration was found to be 5.6×10^{17} cm^{-3}. The hot probe method demonstrated that the films predominantly exhibit p-type conductivity.

Fig. 7, illustrates the fabrication of a chemically synthesised $CuSbS_2$ thin film solar cell with a sequence SLG/Mo/$CuSbS_2$/CdS/Ag. $CuSbS_2$ films act as an absorber layer and chemical bath deposition CdS films [40] serve as the buffer layer in the solar cell. Fig. 8 illustrates the current density-voltage (J-V) characteristics of these thin film solar cells, with analysis conducted under 100 milli watts per sq cm (AM 1.5 irradiation). Table 3 displays cell parameters of $CuSbS_2$ thin film solar cells, fabricated at dissimilar carrier gases.

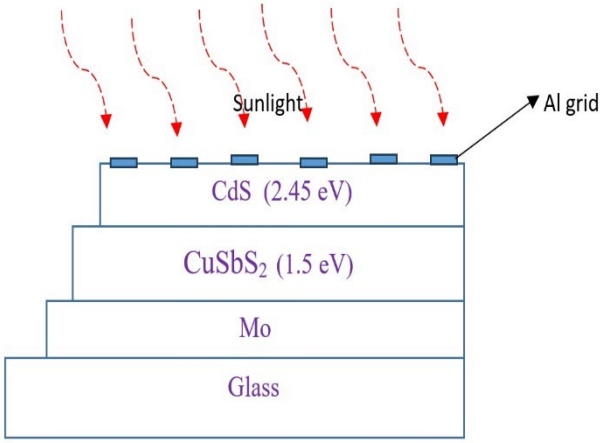

Fig. 7. Sequence heterojunction solar cell.

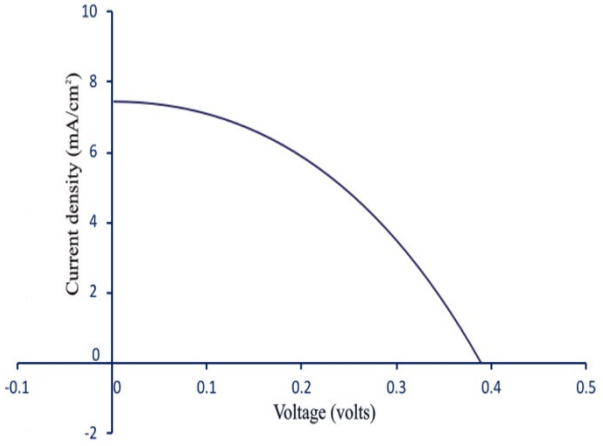

Fig. 8. J-V characteristics of $CuSbS_2$ solar cell.

Table 3. Performance of $CuSbS_2$ solar cells fabricated at two dissimilar carrier gases.

S.No.	Carrier gas	V_{OC} (V)	J_{SC} (mA cm^{-2})	Fillfactor (%)	Efficiency (%)
1	Compressed air	0.14	1.62	--	--
2	Nitrogen	0.39	7.43	20	0.49

The diminished performance might stem from suboptimal parameters, including each layer thickness, the electrical studies of the films, and the limited mobility of charge carriers. Furthermore, the metallurgical interface among the absorber as well as buffer layers is another contributing factor to the efficiency shortfall [41,42]. Nevertheless, the performance cell showed enhancement by using N_2 as the carrier gas.

4. Conclusion

$CuSbS_2$ thin films are effectively fabricated by the conventional spray pyrolysis method with two dissimilar carrier gases. In a spray pyrolytic technique, we are presenting the first-time deposition of $CuSbS_2$ films using N_2 as carrier gas. This study emphasizes the significant influence

of carrier gas on the development of $CuSbS_2$ thin films. Films fabricated using N_2 as a carrier gas have high crystallinity compared to those prepared with other gases. The $CuSbS_2$ films exhibited a chalcostibite structure, with lattice parameters found to be a = 0.5996, b = 0.3802, and c = 1.4506 nm. The band gap value of the films closely matched the optimal performance of the absorber layer in the solar cell when N_2 is used as a carrier gas. $CuSbS_2$ thin film heterojunction solar cells exhibited an efficiency of 0.49%.

References

[1] T. M. Razykov, C. S. Ferekides, D. Morel, E. Stefanakos, H. S. Ullal, H. M. Upadhyaya, Sol. Energy **85**, 1580 (2011); https://doi.org/10.1016/j.solener.2010.12.002
[2] M. Green, E. Dunlop, J. Hohl-Ebinger, M. Yoshita, N. Kopidakis, X. Hao, Prog. Photovolt. **29**(7), 657 (2021); https://doi.org/10.1002/pip.3444
[3] https://www.nrel.gov/pv/interactive-cell-efficiency.html
[4] B. Krishnan, S. Shaji, R. Ernesto, J. Mater. Sci. Mater. Electron. **26**, 4770 (2015); https://doi.org/10.1007/s10854-015-3092-2
[5] D. Colombara, L. M. Peter, K. D. Rogers, J. D. Painter, S. Roncallo, Thin Solid Films **519**, 7438 (2011); https://doi.org/10.1016/j.tsf.2011.01.140
[6] T. Rath, A. J. MacLachlan, M. D. Brown, S. A. Haque, J. Mater. Chem. **3**, 24155 (2015); https://doi.org/10.1039/c5ta05777a
[7] S. Banu, S. Ahn, S. Kyu, Kyunghoon, A. Cho, Sol. Energy Mater. Sol. Cells **151**,14 (2016); https://doi.org/10.1016/j.solmat.2016.02.013
[8] U. Chalapathi, P. U. Bhaskar, S. Sambasivam, Bandar Ali Al-Asbahi, Si-Hyun Park, Heliyon **10**, 27504 (2024); https://doi.org/10.1016/j.heliyon.2024.e27504
[9] S. C. Riha, A. A. Koegel, J. D. Emery, M. J. Pellin, B.F. Martinson, ACS Appl. Mater. Interfaces **9**, 4667 (2017); https://doi.org/10.1021/acsami.6b13033
[10] A. W. Welch, P. P. Zawadzki, S. Lany, C. A. Wolden, A. Zakutayev, Sol. Energy Mater. Sol. Cells **132**, 499 (2015); https://doi.org/10.1016/j.solmat.2014.09.041
[11] V. Vinayakumar, S. Shaji, D. Avellaneda, T. D. Roy, G. Castillo, J. Martinez, B. Krishnan, Sol. Energy Mater. Sol. Cells **164**, 19 (2017); https://doi.org/10.1016/j.solmat.2017.02.005
[12] R. Suriakarthick, V. N. Kumar, T. Shyju, R. Gopalakrishnan, J. Alloys Compd. **651**, 423 (2015); https://doi.org/10.1016/j.jallcom.2015.08.061
[13] W. Septina, S. Ikeda, Y. Iga, T. Harada, M. Matsumura, Thin Solid Films **550**, 700 (2014); https://doi.org/10.1016/j.tsf.2013.11.046
[14] B. Shu, Q. Han, Chalcogenide letters, **13**(2), 46 (2016).
[15]. C. Macías, S. Lugo, Á. Benítez, I. López, B. Kharissov, A. Vázquez, Y. Peña, Mater. Res. Bull. **87**, 161 (2017); https://doi.org/10.1016/j.materresbull.2016.11.028
[16] W. Wang, L. Hao, W. Zhang, Q. Lin, X. Zhang, Z. Tang, J. Mater. Sci., Mater. Electron. **29**, 4075 (2018).
[17] A. Rastogi, N. Janardhana, Thin Solid Films **565**, 285 (2014); https://doi.org/10.1016/j.tsf.2014.06.031
[18] L. Wan, X. Guo, Y. Fang, X. Mao, H. Guo, J. Xu, R. Zhou, J. Mater. Sci. Mater. Electron. **30**, 21485 (2019); https://doi.org/10.1007/s10854-019-02531-2
[19] V. M. Reddy, P. M. Reddy, G. P. Reddy, G. Sreedevi, K. K. Y. B. Reddy, P. Babu, W. K. Kim, K. T. R. Reddy, C. Park, J. Ind. Eng. Chem. **76**, 39 (2019); https://doi.org/10.1016/j.jiec.2019.03.035
[20] Zürich, Thin Film Deposition by Spray Pyrolysis and the Application in Solid Oxide Fuel Cells, 2003.
[21] Y. Zhang, J. Huang, J. Cong, X. Hao, Sol. Energy Mater. Sol. Cells **273**, 112935 (2024); https://doi.org/10.1016/j.solmat.2024.112935
[22] U. Chalapathi, B. Poornaprakash, Chang-Hoi Ahn, Si-Hyun Park, Ceramics International **44**(12), 14844 (2018); https://doi.org/10.1016/j.ceramint.2018.05.117
[23] Y. B. K. Kumar, G. S. Babu, U. Chalapathi, Y. B. Kiran, P. U. Bhaskar, Si-Hyun Park, Physica B **670**, 415366 (2023); https://doi.org/10.1016/j.physb.2023.415366

[24] D. Nagamalleswari, Y. B. K. Kumar, V. Ganesh, Physica B **616**, 413119 (2021); https://doi.org/10.1016/j.physb.2021.413119
[25] Y. Kumar, R. Doddipalli, D. Nagamalleswari, H. Tarigonda, SAE Technical Paper **28**, 573 (2022); https://doi.org/10.4271/2022-28-0573
[26] D. Nagamalleswari, Y. B. K. Kumar, Y. B. Kiran, G. S. Babu, Energy Sources, Part: A Recovery, Util. Environ. Eff. **41**, 3001 (2019); https://doi.org/10.1080/15567036.2019.1583294
[27] Y. B. K. Kumar, D. Nagamalleswari, G. S. Babu, Physica B **645**, 414263 (2022); https://doi.org/10.1016/j.physb.2022.414263
[28] S. Liu, L. Chen, L. Nie, X. Wang, R. Yuan, Chalcogenide Lett. **11**, 639 (2014).
[29] JCPDS Card No. 65–2416.
[30] T. Maeda, T. Wada, Thin Solid Films **582**, 401(2015); https://doi.org/10.1016/j.tsf.2014.11.089
[31] JCPDS Card No.42-0564
[32] D. Perednis, L. J. Gauckler, J. Electroceram. **14**, 103 (2005).
[33] A. Ziti, B. Hartiti, H. Labrim, S. Fadili, H. J. T. Nkuissi, A. Ridah, M. Tahri, P. Thevenin, Appl. Phys. A **125**, 218 (2019); https://doi.org/10.1007/s00339-019-2513-0
[34] M. A. Islam, K. S. Rahman, F. Haque, M. Akhtaruzzaman, M. M. Alam, Z. A. Alothman, K. Sopian, N. Amin, Chalcogenide Lett. **11**, 233 (2014).
[35] H. Gencer, M. Gunes, A. Goktas, Y. Babur, H.I. Mutlu, S. Atalay, J. alloys and compounds **465**, 20 (2008); https://doi.org/10.1016/j.jallcom.2007.10.110
[36] J. Agustin, D. Leonardo, Sadasivan, D. Avellaneda, B. Krishnan, Phys. Status Solidi: C **13**, 24 (2016); https://doi.org/10.1002/pssc.201510102
[37] A. D. Saragih, D.H. Kuo, T.T.A. Tuan, J. Mater. Sci. Mater. Electron. **28**, 2996 (2017); https://doi.org/10.1007/s10854-016-5885-3
[38] N. Katariya, B. Singh, A. Saxena, V. Ganesan, Macromolecular Symposia **407**(1), (2023); https://doi.org/10.1002/masy.202100473
[39] V. G. Rajeshmon, M. R. Rajesh Menon, C. Sudha Kartha, K. P. Vijayakumar, J. Anal. Appl. Pyrol. **110**, 448 (2014); https://doi.org/10.1016/j.jaap.2014.10.014
[40] Y.B. Kumar, V. Raja, Surface Interface **9**, 233 (2017); https://doi.org/10.1016/j.surfin.2017.10.003
[41] Y. Kumar, Y. B. Kiran, H. Tarigonda, R. R. Doddipalli, SAE Technical Paper **28**, 0139 (2023); https://doi.org/10.4271/2023-28-0139
[42] Y. Jayasree, Y. Kumar, G. S. Babu c, P. U. Bhaskar, Physica B **618**, 413199 (2021); https://doi.org/10.1016/j.physb.2021.413199